Results in Optics 7 (2022) 100228

Contents lists available at ScienceDirect

Results in Optics

journal homepage: www.sciencedirect.com/journal/results-in-optics

A novel star-shaped Schiff base compound: Synthesis, properties and application in w-LEDs

Wenyan Fang [b], Zhi Cao [c], Qiman Liu [b], Yihan Chu [b], Hanfei Zhu [b], Weiwei Zhou [b,*], Jiaxiang Yang [a,*]

[a] College of Chemistry & Chemical Engineering, Key Laboratory of Functional Inorganic Materials of Anhui Province, Anhui University, Hefei 230039, PR China
[b] School of Chemistry and Materials Engineering, Huainan Normal University, Anhui, Huainan 232038, PR China
[c] Materials Research Institute of Athlone Institute of Technology, Athlone, Ireland

ARTICLE INFO

Keywords:
α-cyanostilbene derivative
Star-shaped Schiff base
white light-emitting diodes (w-LEDs)

ABSTRACT

A novel star-shaped Schiff base compound (**3**) was designed, synthesized and characterized. The thermal stability of **3** was measured. The photophysical properties and solvent effects of **3** were investigated and further analyzed by density functional theory (DFT). The LEDs of **3** were made, and white light was obtained. The results indicate that as-synthesized compound **3** has high thermal stability, favorable fluorescence emission in both solution and the solid states (i.e. dual-state luminescence), in addition, the solid of **3** may be used for white light-emitting diodes (w-LEDs) due to its favorable fluorescence emission and high thermal stability.

1. Introduction

White light-emitting diodes (w-LEDs) show a lot of merits, such as energy conservation, environmental protection, high luminous efficiency (LE), and long service life, it has increasingly gained popularity in industrial production and human living (Pust et al., 2015). The phosphor-converted w-LED (PC-WLED) is the most popular approach to produce white light. The typical PC-WLED composed of blue chip and yellow phosphor has a simple, compact, and robust architecture featuring a high LE. However, it suffers from a poor color rendering index (CRI) and a cool correlated color temperature (CCT) (Cho et al., 2017). A w-LED with better photometric and colorimetric performances is favorable and desirable. In addition, different applications, e. g. general illumination, backlighting in liquid–crystal displays (LCD), (Li et al., 2018) high-power laser lighting, (You et al., 2021) lamps for greenhouse crop growth, (Li et al., 2020) exert different requirements on the emission position and profile of the phosphors. Therefore, numerous efforts are dedicated to developing highly efficient red/green/blue/yellow phosphors compatible with the blue/near-ultraviolet LED chips (Wang et al., 2018; Ye et al., 2010).

Even if an abundance of phosphors were exploited extensively with various spectral features in the past few years, they could be classified into two categories based on containing rare-earth (RE) elements or not. The former serves as the commercial mainstream products at the present stage. The classic representatives are red $CaAlSiN_3:Eu^{2+}$, green β-sialon: Eu^{2+} and yellow YAG:Ce^{3+} phosphors (Xia and Liu, 2016). Although excellent in comprehensive performance, they may encounter potential economic and environmental pressures induced from the process of mining and refining of the nonrenewable RE. Keeping it in mind, it is of great significance to seek alternatives with eco-friendliness, low cost and superior performance. The RE-free phosphors under consideration so far mainly involve the Mn^{4+}/Mn^{2+}-activated inorganic materials, (Zhou et al., 2018; Zhou et al., 2019) quantum dots (QD), (Won et al., 2019; He et al., 2020) perovskite, (Shao et al., 2019) organic (Kundu et al., 2020) and polymer luminescent materials; (Kim et al., 2020) as well as metal–organic frameworks (MOF) (Wang et al., 2019; Lustig et al., 2020). Tremendous progress was achieved for these materials in recent years, and the preliminary device performances were demonstrated (Zhang et al., 2021).

Compared with other materials, organic photoelectric functional materials have special advantages, such as definite molecular structure, easy to tailor, modify, functionalize, and high luminous efficiency, tunable photoelectronic properties, simple manufacturing process, easy purification processes, low cost and so on (Kundu et al., 2020; Liao et al., 2020; Yuan et al., 2018; Zhang et al., 2018; Naqvi et al., 2021; Shen et al., 2020). Besides the advantages above, organic LEDs are glare-free. They can provide exceedingly homogenous illumination (Gather et al., 2011). Hence, it is of great significance to synthesize organic

* Corresponding authors.
E-mail address: jxyang@ahu.edu.cn (J. Yang).

https://doi.org/10.1016/j.rio.2022.100228
Received 10 December 2021; Received in revised form 2 February 2022; Accepted 6 March 2022
Available online 8 March 2022

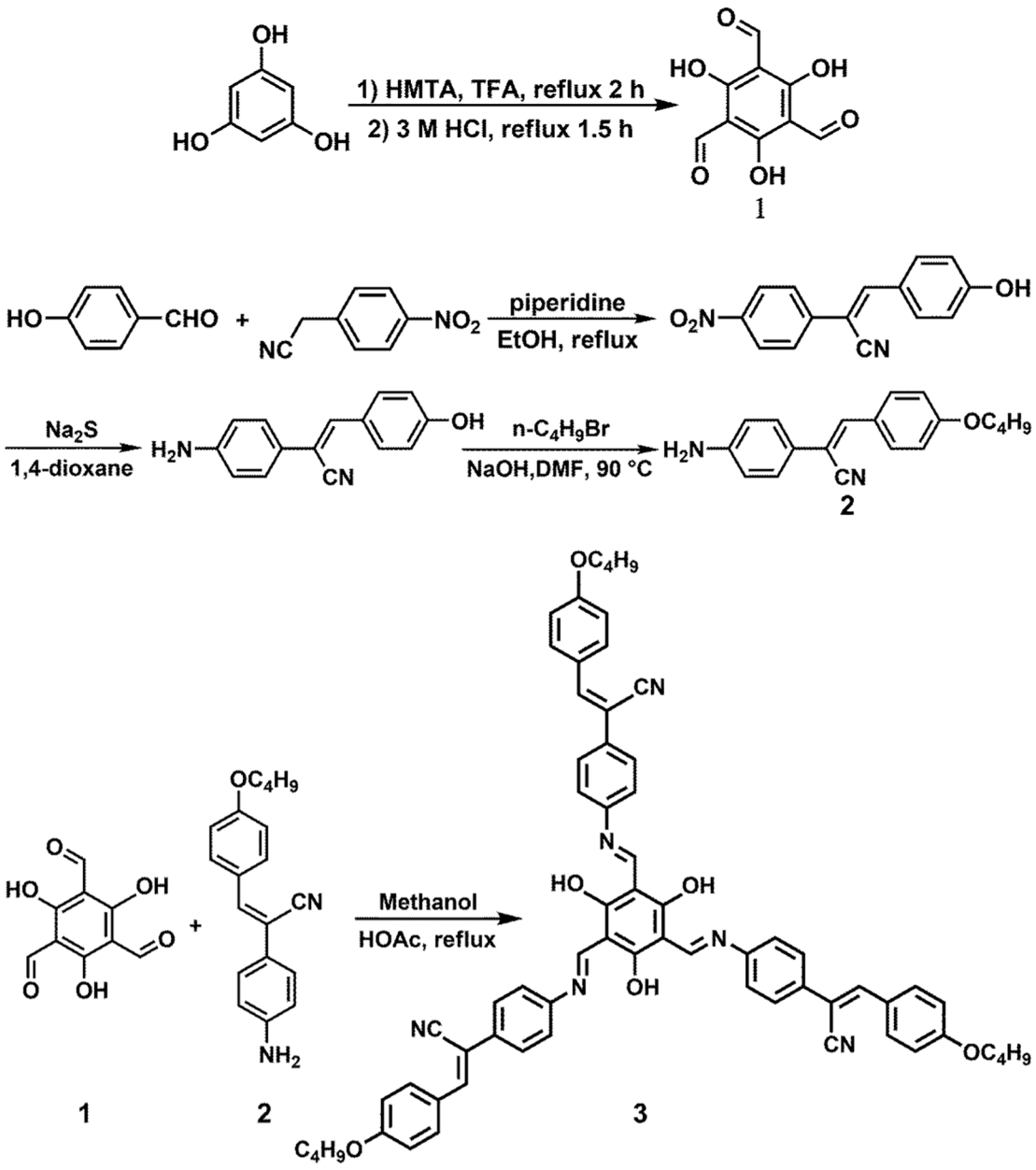

Scheme 1. The synthesis routes of compounds **1**–**3**.

luminescent materials from low-cost raw materials to apply in w-LEDs by mild condition and simple operation course. Among organic compounds, Schiff bases are a category of compounds containing C═N groups. A variety of Schiff bases can be easily synthesized from a condensation reaction between different carbonyl compounds and primary amines. Schiff bases have many advantages, such as easy synthesis, robustness against light and chemicals, remarkable photophysical properties. It can be used as a pigment, dye, fluorescent probes, electroluminescent devices, light-harvesting materials, and it can also be used as an intermediate to generate various derivatives (Kushwah et al., 2019; Deng et al., 2020; Weng et al., 2020). However, the application of Schiff bases in w-LED is rarely reported (Fang et al., 2018; Beata et al., 2020). Thus, in this paper, an organic small molecule compound **3** (a star-shaped α-cyanostilbene derivative Schiff base) was designed, synthesized and characterized by ^{1}H NMR, MS and FT-IR. The thermal stability, optical performance and application in w-LEDs of **3** were studied.

2. Experimental

2.1. Synthesis

The synthesis routes of intermediates (**1**, **2**) and target product (**3**) are presented in Scheme 1.

2.1.1. Synthesis of 1 and 2

Intermediate **1** (triformylphloroglucinol) was synthesized by Duff's reaction according to the literature method (Chong et al., 2003; Lu et al., 2014). FT-IR (KBr, ν/cm^{-1}): 2920, 2897, 2851, 1643, 1599, 1433, 1390, 1255, 1193.26, 1151, 968, 874, 819, 786, 608 (shown in Fig. S1). Intermediate **2** was synthesized by three steps as follow (Gupta et al., 2018): Firstly, the 3-(4-hydroxyphenyl)-2-(4-nitrophenyl) acrylonitrile was synthesized by a typical Knoevenagel reaction from 4-hydroxybenzaldehyde and 4-nitrophenylacetonitrile with the piperidine catalyst, then the nitro group was reduced to an amino group *via* a reduction reaction by using Na_2S in 1,4-dioxane. Lastly, intermediate **2** was

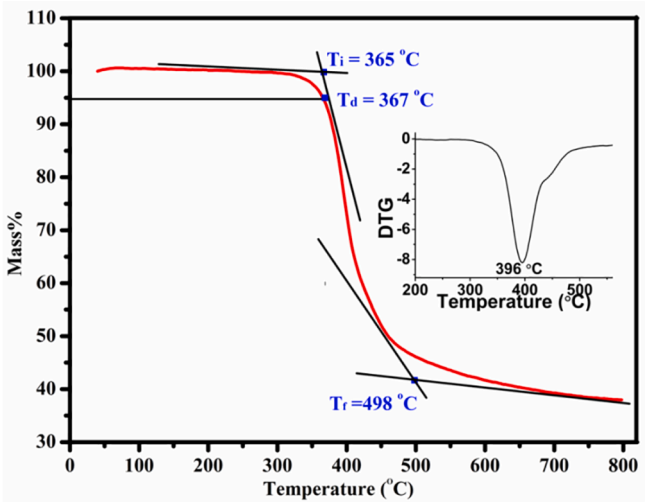

Fig. 1. The TGA curve of **3** recorded under a nitrogen atmosphere at a heating rate of 10 °C · min^{-1}. Inset is DTG curves.

synthesized utilizing a typical Williamson reaction from 2-(4-aminophenyl)-3-(4-hydroxyphenyl) acrylonitrile and 1-butylbromide in DMF and NaOH.

2.1.2. Synthesis and characterization of target product 3

Target compound **3** was easily prepared by the Schiff-base reaction (Jia and Li, 2015) from compounds **2** and **1** in absolute methanol using a catalytic amount of HOAc. The specific steps are as the following steps: Compound **1** (0.10 g, 0.48 mmol), **2** (0.46 g, 1.57 mmol) and three drops of glacial acetic acid were added in absolute methanol (20 mL). The mixture was stirred under reflux for about 48 h. Reaction progress was detected by thin-layer chromatography (TLC). The resulting solution was cooled to room temperature and then was filtered. The precipitate was washed several times with methanol and dried under vacuum. Finally, the yellowish solid target product **3** was obtained (0.37 g, yield: 75%). FT-IR (KBr, ν/cm^{-1}): 2955, 2930, 2869, 2213, 1620, 1565, 1508, 1453, 1283, 1235, 1175, 998, 829, 583, 531 (result is shown in Fig. S1). ^{1}H NMR (400 MHz, $CDCl_3$, δ in ppm): 0.98–1.04 (m, 9H), 1.41–1.54 (m, 6H), 1.67–1.78 (m, 5H), 3.58–4.03 (m, 7H), 6.46–7.25 (m, 20H), 7.42–8.33 (m, 10*H*), 12.41–13.00 (m, 3H) (as shown in Fig. S2). MALDI-TOF-MS: m/z = 1033.212 (M + H), calc'd for $C_{66}H_{60}N_6O_6$ = 1032.219 (M) (as shown in Fig. S3). It can be seen in Fig. S2 that the chemical shift of Schiff base **3** is more complex at 6–9 ppm and 12–14 ppm. This may result from the presence of keto-enol tautomer and the cis (Z) – trans (E) isomers of the C═C bond (Atzin-Macedo et al., 2020; Zbačnik et al., 2017; Ogawa et al., 1998; Cembran et al., 2004). Compound **3** was found to be soluble easily in common organic solvents, such as benzene, tetrahydrofuran (THF) and chloroform, but is insoluble in ethanol, petroleum ether and water.

Table 1
Photophysical parameters of compound **3** in various solvents.

Compound	Solvents	λ_{ab} [a]	λ_{em} [b]	k ($\times 10^4$) [c]	$\Delta\nu$ [d]	Δf [e]
3	benzene	438	493	13.28	2547	0.0026
	DCM	436	491	14.19	2569	0.2185
	THF	434	492	13.77	2558	0.2097
	EA	430	487	14.62	2722	0.1997
	ethanol	429	529	8.05	4406	0.2903
	AN	426	489	8.76	3024	0.3055
	DMF	437	493	13.93	2599	0.2751

[a] The wavelength of the maximum absorption. [b] The wavelength of the maximum emission, excited using the absorption maximum 434 nm, [c] Extinction coefficient (L · mol^{-1} · cm^{-1}), [d] Stokes' shift (cm^{-1}), [e] orientation polarizability.

3. Results and discussion

3.1. 1. Thermal property

It is common knowledge that good thermal stability is conducive to the application of organic materials. To estimate the thermal stability of **3**, thermogravimetric analysis (TGA) was performed under a nitrogen atmosphere at a heating rate of 10 °C min^{-1}, as presented in Fig. 1. It is clear that weight loss of **3** locates in the range of 365–498 °C, the temperature of 5% weight loss (T_d) is at 367 °C, and the quickest decomposition temperature occurs at 396 °C (Kong et al., 2013; Fang et al., 2017). The above data indicate that **3** possesses high thermal stability and is suitable for application in optical devices.

3.2. Optical properties

The photophysical properties of the THF solution and the solid of **3** were evaluated, respectively. The spectra of UV–vis absorption and fluorescence are presented in Fig. 2. As seen in Fig. 2b, the target compound **3** possesses fluorescence emission in both the solution and solid states. The absolute emission quantum yields (Φ_F) are 15.33% and 2.11%, respectively (Fig. S5–6). The maximum emission peaks locate at 492 nm and 571 nm, respectively. The emission wavelength maxima of solid **3** exhibits a considerable bathochromic effect of 79 nm compared with the one of **3** in solution. It is probably because the appropriate molecular packing mode of solid **3** restricts the intramolecular rotation and enhances the degree of the conjugation.

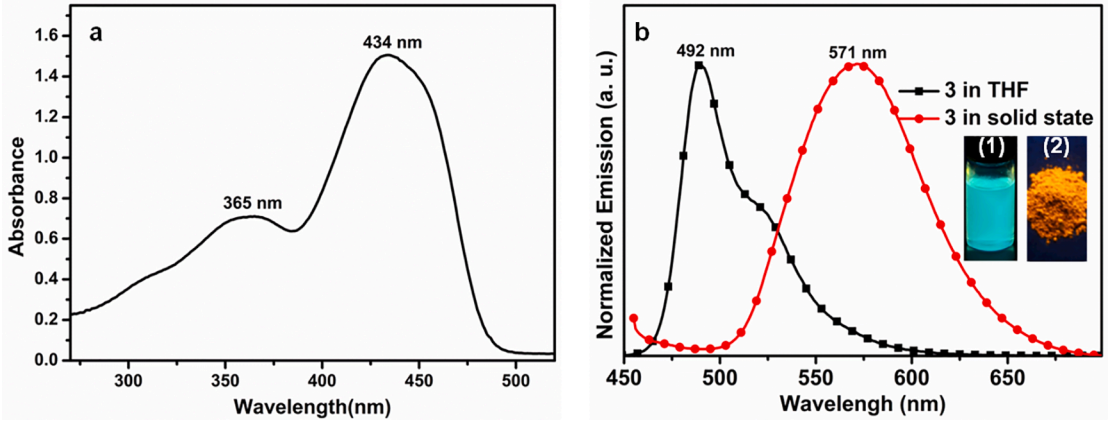

Fig. 2. (a) UV–vis and (b) emission spectra of **3** in THF solution (c = 1.0 × 10^{-5} M) and in the solid-state, excitation wavelength using the maximum absorption 434 nm. The inset in (b) represents the fluorescence photographs of **3** in THF solution (1) and in the solid-state (2) under irradiation of 365 nm UV lamp.

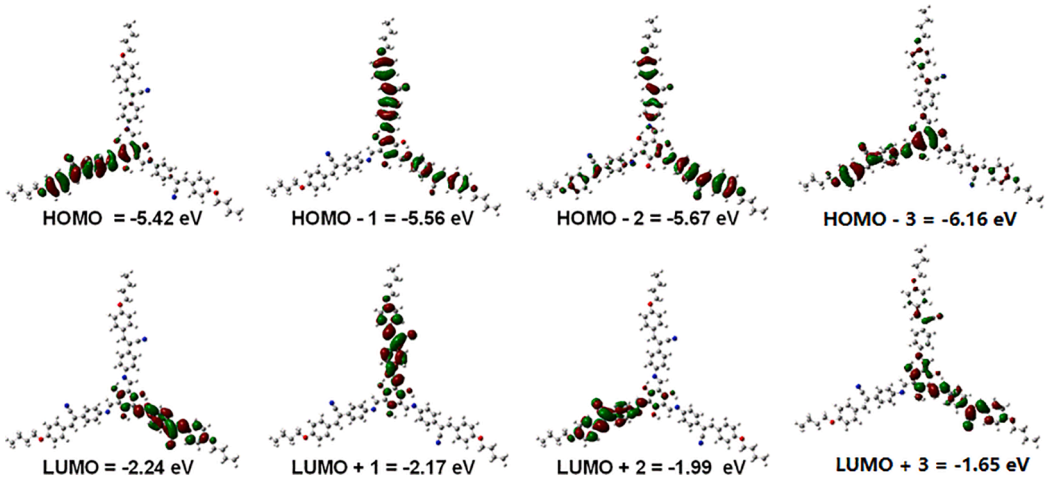

Fig. 3. The frontier molecular orbital levels and electron clouds distribution of compound **3**.

As seen in Fig. 2a, two obvious absorption peaks are appeared at 365 nm and 434 nm, respectively. The values of the extinction coefficients (k) of the two absorption peaks are both higher than 1×10^4 L · cm^{-1} · mol^{-1} (Table 1), which suggests that the electron transition of **3** is permitted. For a deeper understanding of the absorbing behavior of **3**, theoretical calculations were performed using the density functional theory (DFT). Geometry optimizations and electronic properties of compound **3** were carried out at a theoretical level of the B3LYP/6-31G (d), and the electronic excitations related to the absorption spectra of the compound were performed using the time-dependent-DFT (TD-DFT) (Frisch et al., 2009). Among keto-enol tautomer and E-Z isomers, the enol structure is the most stable from the calculated results of model compounds (As can be seen in Fig. S4). The experimental and calculated values of the maximum absorption (λ_{max}), oscillator strengths, and the major contributions of orbital and HOMO-LUMO energy gaps are presented in Table S1, respectively. The calculated maximum absorptions of **3** are 359 nm and 435 nm respectively, which is nicely consistent with the experimental result (365 nm and 434 nm) of the absorption spectrum. From the investigations of the frontier molecular orbital (FMO) energy levels, the corresponding absorption band at the 365 nm is predicted to be a joint contribution combination of two electronic transition modes, H → L + 3 (65.8%) and H − 2 → L + 2 (12.6%), the band at the 434 nm is contribution combination of H → L (61.3%) and H − 2 → L (10.6%), which are probably attributed to the sum of π-π* and

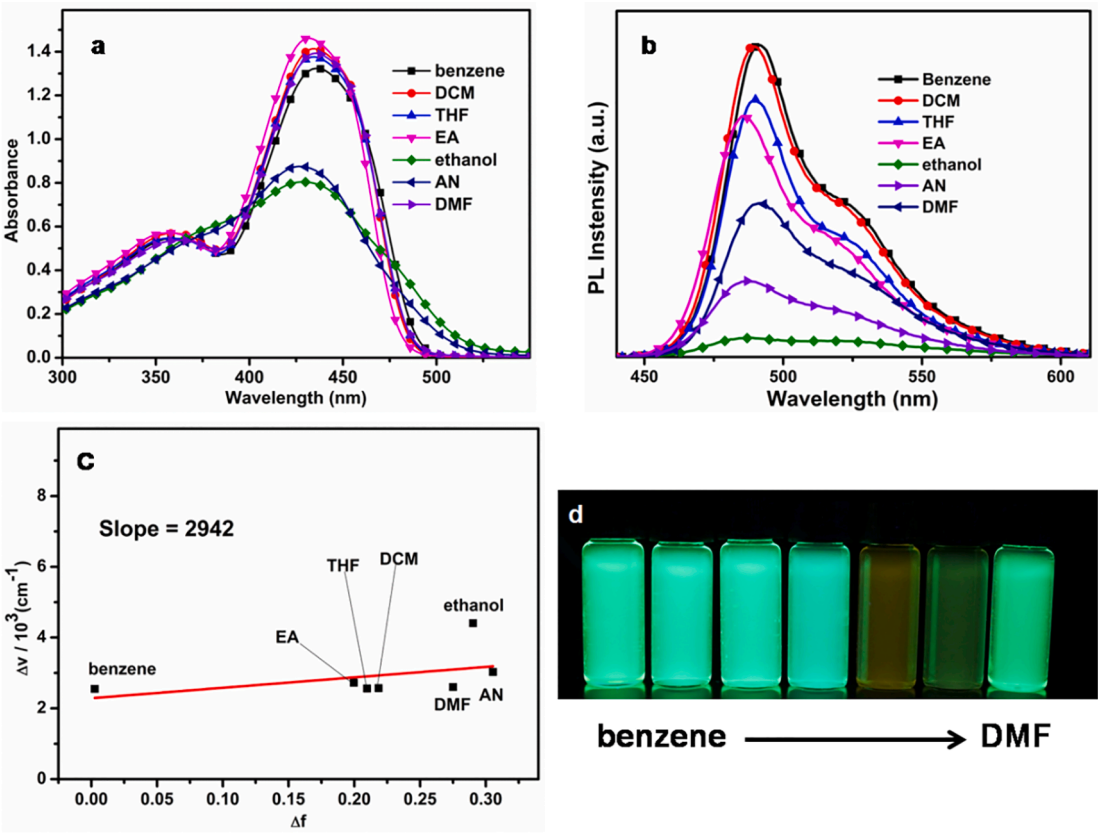

Fig. 4. UV–vis (a) and emission (b) spectra, solution concentration are all 1.0×10^{-5} M, excitation wavelength using the maximum absorption 434 nm. Lippert-Mataga plot of compound **3** in different polarities solvents (c). Photograph of the fluorescence variation of **3** taken under UV irradiation in different solvents (d).

intramolecular charge transfer (ICT) transition, while the absorption peak at 365 nm corresponds to π-π* transition (Naqvi et al., 2021; Zhang et al., 2018; Bucinskas et al., 2015) photophysical properties of the THF To further understand the ICT processes, the DFT calculations were also used to research the electron cloud distributions of ground and excited states (Fig. 3). As shown in Fig. 3, as the main contribution FMO H → L of 434 nm, the electron cloud of the highest occupied molecular orbital (HOMO) is mainly distributed on the one branch of conjugated moieties formed connecting the central benzene ring and α-cyano-substituted stilbene by C═N. The electron cloud of the lowest unoccupied molecular orbital (LUMO) is very concentrated on one α-cyano-substituted stilbene moieties because of the strong electron-withdrawing ability of –CN, less distributed on the central benzene ring, and as the main contribution FMO H → L + 3 of 365 nm, the distribution of electron cloud on H and L + 3 is essentially the same, electron transfer is almost nonexistent. It indicates that compound **3** has a weak intramolecular charge transfer (ICT) effect.

3.3. Solvent effect

It is well known that absorption and emission spectra can be affected by the surrounding medium. The polarity of solvent can lead to the change in intensity, maximum wavelength and shape of spectra. This phenomenon is known as solvatochromism (Galer et al., 2014). Thus, the impacts of polarities on the optical properties of **3** in several various solvents were examined. The spectra of absorption and emission, Lippert-Mataga plot, and photograph of solvatochromism are given in Fig. 4. The Lippert-Mataga plot relates stokes shift (Δυ) according to Eq. (1). Where υ_{ab} and υ_{em} are the wavenumbers (cm^{-1}) of the absorption and emission, respectively; Δf is solvent polarity parameters; h, c and a represent Planck's constant, the velocity of light and the Onsager radius, respectively; $\Delta\mu = \mu_e - \mu_g$ is the dipole moment difference between the ground and excited states. The values of Δf were obtained through equation (2). Where ε and n are the dielectric constant and refractive index of the medium, respectively.

The measured photophysical parameters, the calculated Stokes' shift (Δυ) and the solvent polarity parameters (Δf) are summarized in Table 1. From Fig. 4a and Table 1, there are two similar absorption peaks at about 360 nm and 430 nm of **3** in benzene, dichloromethane (DCM), THF, ethyl acetate (EA) and N,N-dimethylformamide (DMF), While **3** in ethanol and acetonitrile (AN), the fine structure of the absorption band almost disappeared and formed a broad peak, the extinction coefficient greatly reduced, and absorption peaks have a small blue shift. This may be due to the stronger interaction between the solvent and the solute molecules, when **3** is in strongly polar solvents (Hu et al., 2009; Zheng et al., 2019; Feng et al., 2020). For fluorescence spectra (Fig. 4b), the shift of emission peaks is small indicating a weak the ICT character of the compound **3**. The emission intensity decreases with increasing polarity of solvent, especially the solution of **3** in ethanol or AN. We presume that aggregation or complexes may be formed due to low solubility, although apparently transparent and particle-free of **3** in highly polar media (Hu et al., 2009), and the molecule of **3** may undergo the change of conformation or the ratio of different isomers duo to the weak interaction of N···H or O···H.) (Atzin-Macedo et al., 2020; Zheng et al., 2019; Feng et al., 2020) In addition, the Lippert-Mataga plot of Δυ against Δf exhibits an upward straight line with some slope (Fig. 4c), which implies that the dipole moment in the excited-state is greater than the value in corresponding ground-state, and a weak ICT feature (Evecen et al., 2016; Awuah et al., 2011; Hariharan et al., 2015; Yang et al., 2013; Jiménez-Sánchez et al., 2015).

4. Electroluminescence

To validate the application potentiality of the **3** in solid-state lighting devices, a LED was fabricated by integrating the **3** with the blue LED chips. The **3** was mixed homogenously with epoxy resin, coated on the

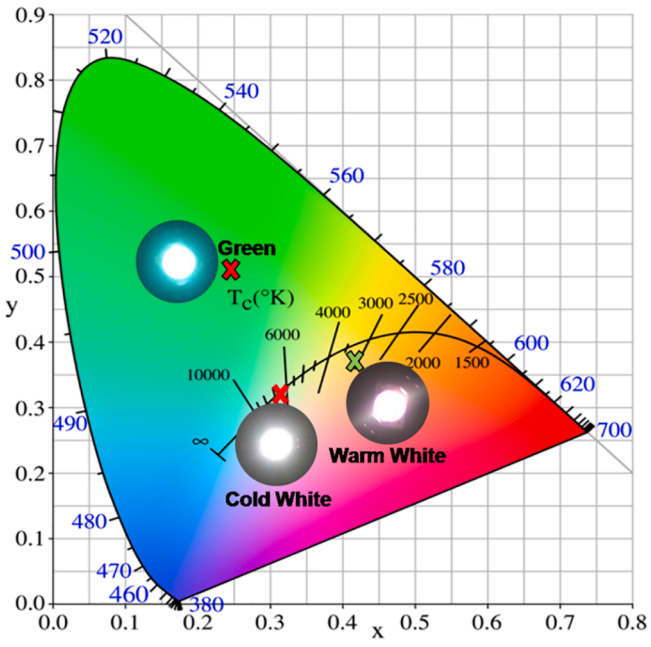

Fig. 5. CIE1931 chromaticity coordinates of the constructed LEDs. The insets are the photographs of LED devices with a forward current of 50 mA.

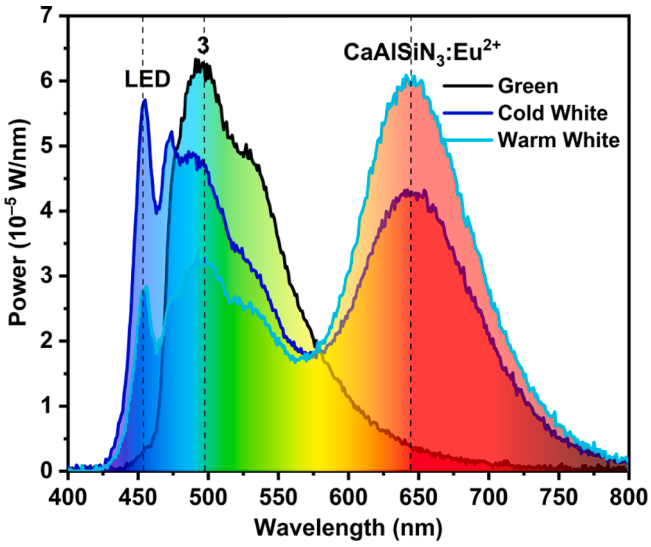

Fig. 6. The EL spectra of the constructed LEDs upon the driving current of 50 mA.

Table 2
The EL parameters of the constructed LEDs upon driving current of 50 mA.

Composition	CIE 1931	LE / lm/W	CRI / %	CCT / K	Color
20 G: 0 R*	(0.2473, 0.5072)	32.21	29.9	7515	Green
20G: 50 R	(0.3177, 0.3255)	29.39	64.4	6255	Cold White
20G: 70R	(0.4127, 0.3658)	28.89	59.9	3116	Warm White

*G:R denotes the amounts of sample 3 (G) and $CaAlSiN_3:Eu^{2+}$ red phosphor (R) in units of mg.

Table 3
The device parameters under different driving currents.

Current / mA	*x*	*y*	LE / Lm/W	CRI / %	CCT / K
25	0.3181	0.3261	30.62	64.0	6233
50	0.3177	0.3255	29.39	64.4	6255
75	0.3171	0.3242	27.62	64.3	6297
100	0.316	0.3233	26.39	64.7	6363
125	0.3156	0.3221	25.24	64.5	6392
150	0.315	0.3206	24.22	64.4	6442
175	0.3145	0.3195	23.33	64.3	6476
200	0.3135	0.3174	22.40	63.9	6557

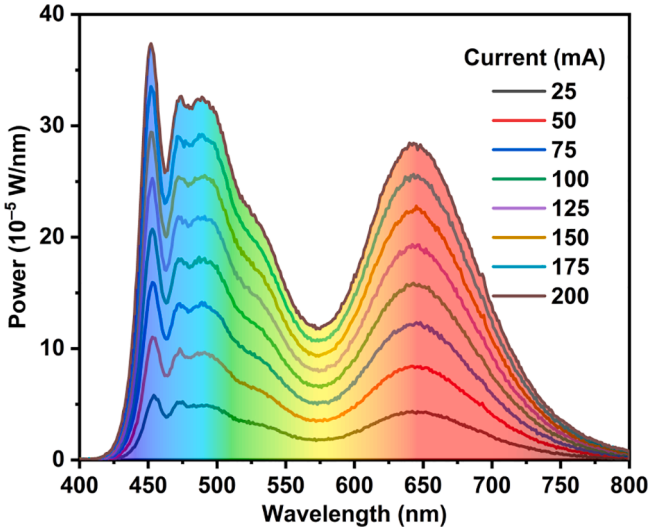

Fig. 7. The EL spectral evolution of the constructed LEDs as a function of the driving currents.

455 nm chips, and finally solidified in a drying oven at 150 °C for 2 h. The LED emitted bright green light, which was observed by naked eyes and confirmed by the CIE1931 chromaticity coordinates of (0.2473, 0.5072), as shown in Fig. 5. The LE reaches up to 32.21 lm/W.

To achieve white light, a certain amount of commercial $CaAlSiN_3$:Eu^{2+} red phosphor was further added to compensate for the lacking red component. In this case, the electroluminescent spectra presented in Fig. 6 were mainly composed of three emissions originating in the blue LED, green **3** and red $CaAlSiN_3$:Eu^{2+} phosphor, respectively. Table 2 lists the relevant parameters of LEDs. The cold and warm white lights were realized by tailoring the amount of **3** and red phosphor (Fig. 5), revealing the feasibility of the **3** in PC-WLED applications. The former exhibits the CCT of 6255 K, CRI of 64.4% and LE of 29.39 lm/W, while the latter has CCT of 3116 K, CRI of 59.9% and LE of 28.89 lm/W. Unsurprisingly, the increment in the ratio of Red-Green gives rise to slightly lower LE, as the red emission at around 650 nm is on the edge of photopic vision of human eyes. The LE is comparable to diphenylfumaronitrile core-based dyes (29–40 lm/W), (Wu et al., 2020) and is significantly greater than carbon dots/Zr-MOF nanocomposite (1.7 lm/W) (Wang et al., 2019) (see Table 3).

Moreover, the device is driven under a series of driven currents of 25–200 mA to monitor the performance variation. Fig. 7 indicates that higher current contributes to a higher power and thus more intense emissions. The LE is inevitably reduced from 30.62 lm/W to 22.4 lm/W because of the efficiency drop of blue chips at high current density. However, the whole EL profiles keep nearly unchanged. The variations of CIE1931 coordinate *x* and *y* are only 0.0046 and 0.0087, respectively. The CRI shows a slight fluctuation between 63.9% and 64.7%. These subtle changes confirm the excellent color stability of the packaged LEDs. Therefore, the **3** can be regarded as a promising candidate color converter for the high-power solid-state lighting devices.

5. Conclusions

In conclusion, a novel star-like α-cyanostilbene derivative-Schiff base compound **3** was designed and successfully synthesized through a simple method. Thermogravimetric analysis indicated that compound **3** exhibits high thermal stability. The investigation of theoretical calculation and solvent effect revealed that the enol structure is the most stable form among keto-enol tautomer and E-Z isomers of **3**, and a weak intramolecular charge transfer (ICT) characteris present in compound **3**. In addition, **3** can be used to fabricate white light-emitting diodes (w-LEDs) due to its satisfactory fluorescence emission and high thermal stability. We expect our work would be valuable for the design and synthesis of new fluorescent materials with dual-state luminescence. We believe our research also provides idea and method for developing alternative material of RE-free phosphors for the application in w-LEDs.

Declaration of Competing Interest

The authors declare that they have no known competing financial interests or personal relationships that could have appeared to influence the work reported in this paper.

Acknowledgments

This work was supported by the Natural Science Foundation of the Anhui Higher Education Institutions of China (No. KJ2020A0650) and . the National Natural Science Foundation of China (51673001).

Appendix A. Supplementary data

Supplementary data to this article can be found online at https://doi.org/10.1016/j.rio.2022.100228.

References

Pust, P., Schmidt, P.J., Schnick, W., 2015. A revolution in lighting. Nat. Mater. 14 (5), 454–458.
Cho, J., Park, J.H., Kim, J.K., Schubert, E.F., 2017. White light-emitting diodes: History, progress, and future. Laser Photonics Rev. 11 (2), 1600147.
Li, S.X., Wang, L., Tang, D.M., Cho, Y.J., Liu, X.J., Zhou, X.T., Lu, L., Zhang, L., Takeda, T., Hirosaki, N., Xie, R.J., 2018. Achieving high quantum efficiency narrow-band β-sialon:Eu^{2+} phosphors for high-brightness LCD backlights by reducing the Eu^{3+} luminescence killer. Chem. Mater. 30, 494–505.
You, S.H., Li, S.X., Wang, L., Takeda, T., Hirosaki, N., Xie, R.J., 2021. Ternary solid solution phosphors Ca 1-x-y Li x Al 1-x-y Si 1+x+y N 3-y O y : Ce 3+ with enhanced thermal stability for high-power laser lighting. Chem. Eng. J. 404, 126575.
Li, L., Tian, G., Chang, W.X., Yan, Y.L., Ling, F.L., Jiang, S., Xiang, G.T., Zhou, X.J., 2020. A novel double-perovskite LiLaMgTeO6:Mn^{4+} far-red phosphor forindoor plant cultivation white LEDs: crystal and electronic structure, and photoluminescence properties. J. Alloy. Compd. 832, 154905.
Wang, L., Xie, R.J., Suehiro, T., Takeda, T., Hirosaki, N., 2018. Down-conversion nitride materials for solid state lighting: recent advances and perspectives. Chem. Rev. 118, 1951–2009.
Ye, S., Xiao, F., Pan, Y.X., Ma, Y.Y., Zhang, Q.Y., 2010. Phosphors in phosphor-converted white light-emitting diodes: Recent advances in materials, techniques and properties. Mat. Sci. Eng. R 71 (1), 1–34.
Xia, Z.G., Liu, Q.L., 2016. Progress in discovery and structural design of color conversion phosphors for LEDs. Prog. Mater. Sci. 84, 59–117.
Zhou, Q., Dolgov, L., Srivastava, A.M., Zhou, L., Wang, Z.L., Shi, J.X., Dramićanin, M.D., Brik, M.G., Wu, M.M., 2018. Mn^{2+} and Mn^{4+} red phosphors: synthesis, luminescence and applications in WLEDs. A review. J. Mater. Chem. C 6, 2652–2671.
Zhou, G., Jiang, X., Molokeev, M., Lin, Z., Zhao, J., Wang, J., Xia, Z., 2019. Optically modulated ultra-broad-band warm white emission in Mn^{2+}-doped ($C_6H_{18}N_2O_2$) PbBr 4 hybrid metal halide phosphor. Chem. Mater. 31 (15), 5788–5795.
Won, Y.-H., Cho, O., Kim, T., Chung, D.-Y., Kim, T., Chung, H., Jang, H., Lee, J., Kim, D., Jang, E., 2019. Highly efficient and stable InP/ZnSe/ZnS quantum dot light-emitting diodes. Nature 575 (7784), 634–638.
He, P., Shi, Y., Meng, T., Yuan, T., Li, Y., Li, X., Zhang, Y., Fan, L., Yang, S., 2020. Recent advances in white light-emitting diodes of carbon quantum dots. Nanoscale 12 (8), 4826–4832.
Shao, G., Zhao, Y., Yu, Y., Yang, H., Liu, X., Zhang, Y., Xiang, W., Liang, X., 2019. Bright emission and high photoluminescence $CsPb_2Br$ 5NCs encapsulated in mesoporous

silica with ultrahigh stability and excellent optical properties for white light-emitting diodes. J. Mater. Chem. C 7 (43), 13585–13593.
Kundu, S., Sk, B., Pallavi, P., Giri, A., Patra, A., 2020. Molecular engineering approaches towards all-organic white light emitting materials. Chem. Eur. J. 26 (25), 5557–5582.
Kim, J., Lee, J., Lee, T.S., 2020. Size-dependent fluorescence of conjugated polymer dots and correlation with the fluorescence in solution and in the solid phase of the polymer. Nanoscale 12 (4), 2492–2497.
Wang, Z., Zhu, C.-Y., Mo, J.-T., Fu, P.-Y., Zhao, Y.-W., Yin, S.-Y., Jiang, J.-J., Pan, M., Su, C.-Y., 2019. White-Light Emission from dual-way photon energy conversion in a dye-encapsulated metal-organic framework. Angew. Chem. Int. Ed. 58 (29), 9752–9757.
Lustig, W.P., Shen, Z., Teat, S.J., Javed, N., Velasco, E., O'Carroll, D.M., Li, J., 2020. Rational design of a high-efficiency, multivariate metal-organic framework phosphor for white LED bulbs. Chem. Sci. 11 (7), 1814–1824.
Zhang, H., Zhang, H.Q., Pan, A.Z., Yang, B., He, L., Wu, Y.S., 2021. Rare earth-free luminescent materials for WLEDs: recent progress and perspectives. Adv. Mater. Technol. 6, 2000648.
Liao, Q., Kang, Q., Yang, Y., An, C.B., Xu, B.W., Hou, J.H., 2020. Tailoring and modifying an organic electron acceptor toward the cathode interlayer for highly efficient organic solar cells. Adv. Mater. 32, 1906557.
Yuan, H., Li, M.-Y., Chen, C.-N., Zhang, Y., Liu, W.-Q., 2018. Substituent effects on the UV absorption energy of 2,5-disubstituted pyrimidines. J. Phys. Org. Chem. 31 (10), e3860.
Zhang, Y.H., Mao, H.L., Xu, W.Q., Shi, J.B., Cai, Z.X., Tong, B., Dong, Y.P., 2018. Aggregation-induced emission of multiphenyl-substituted 1,3-butadiene derivatives: synthesis, properties and application. Chem. Eur. J. 24, 1–14.
Naqvi, S., Chaudhary, N., Singhal, S., Yadav, P., Patra, A., 2021. Hole transport materials by direct C-H arylation for organic solar cells: effect of structure and conjugation on electrical, optical and computational properties. ChemistrySelect 6, 131–139.
Shen, H., Li, Y., Li, Y., 2020. Self-assembly and tunable optical properties of intramolecular charge transfer molecules. Aggregate 1 (1), 57–68.
Gather, M.C., Köhnen, A., Meerholz, K., 2011. White organic light-emitting diodes. Adv. Mater. 23 (2), 233–248.
Kushwah, N., Mula, S., Wadawale, A.P., Joshi, M., Gotluru, K., Kumar, M., Ghanty, T.K., Nayak, S.K., Jain, V.K., 2019. Synthesis and characterization of some BODIPY-based substituted salicylaldimine schiff bases. J. Heterocyclic Chem. 56 (9), 2499–2507.
Deng, H.-H., Huang, K.-Y., He, S.-B., Xue, L.-P., Peng, H.-P., Zha, D.-J., Sun, W.-M., Xia, X.-H., Chen, W., 2020. Rational design of high-performance donor-linker-acceptor hybrids using a schiff base for enabling photoinduced electron transfer. Anal. Chem. 92 (2), 2019–2026.
Weng, Q.H., Yi, J.Q., Chen, X.P., Luo, D.W., Wang, Y.D., Sun, W.M., Kang, J., Han, Z.Z., 2020. Controllable synthesis and biological application of schiff bases from D-glucosamine and terephthalaldehyde. ACS Omega 5, 24864–24870.
Fang, W.Y., Zhao, W., Pei, P., Liu, R., Zhang, Y.Y., Kong, L., Yang, J.X., 2018. A ʌ-shaped cyanostilbene derivative: multi-stimuli responsive fluorescence sensors, rewritable information storage and colour converter for w-LEDs. J. Mater. Chem. C 6, 9269–9276.
Beata, D.Z., Magdalena, B., Christophe, C., Georges, B., 2020. Nonlinear optical study of Schiff bases using Z-scan technique. Opt. Laser Technol. 124, 105968.
Chong, J.H., Sauer, M., Patrick, B.O., MacLachlan, M.J., 2003. Highly stable keto-enamine salicylideneanilines. Org. Lett. 5 (21), 3823–3826.
Lu, H.B., Qiu, L.Z., Zhang, G.Y., Ding, A.X., Xu, W.B., Zhang, G.B., Wang, X.H., Kong, L., Tian, Y.P., Yang, J.X., 2014. Electrically switchable photoluminescence of fluorescent-molecule-dispersed liquid crystals prepared via photoisomerization-induced phase separation. J. Mater. Chem. C 2, 1386–1389.
Gupta, R.K., Pathak, S.K., De, J., Pal, S.K., Achalkumar, A.S., 2018. Room temperature columnar liquid crystalline self-assembly of acidochromic, luminescent, star-shaped molecules with cyanovinylene chromophores. J. Mater. Chem. C 6 (7), 1844–1852.
Jia, Y., Li, J.B., 2015. Molecular assembly of schiff base interactions: construction and application. Chem. Rev. 115, 1597–1621.
Atzin-Macedo, C.M., Pastor-Ramírez, C., González-Peláez, R., Pérez-Flores, F.J., Hernández-Anzaldo, S., Vazquez-Lima, H., Reyes-Ortega, Y., 2020. Tautomeric study of schiff bases derived from o-dihydroxybenzaldehyde by UV-Vis, IR, ^{1}H NMR, ^{13}C NMR spectroscopy and computational modeling. ChemistrySelect 5 (36), 11120–11126.
Zbačnik, M., Pičuljan, K., Parlov-Vuković, J., Novak, P., Roodt, A., 2017. Four thermochromic o-hydroxy schiff bases of α-aminodiphenylmethane: solution and solid state study. Crystals 7 (1), 25.
Ogawa, K., Kasahara, Y., Ohtani, Y., Harada, J., 1998. Crystal structure change for the thermochromy of N-Salicylideneanilines. The first observation by X-ray diffraction. J. Am. Chem. Soc. 120 (28), 7107–7108.
Cembran, A., Bernardi, F., Garavelli, M., Gagliardi, L., Orlandi, G., 2004. On the mechanism of the cis-trans isomerization in the lowest electronic states of azobenzene: S 0, S1, and T1. J. Am. Chem. Soc. 126, 3234–3243.
Kong, L., Yang, J.X., Zhou, H.P., Li, S.L., Hao, F.Y., Zhang, Q., Tu, Y.L., Wu, J.Y., Xue, Z. M., Tian, Y.P., 2013. Synthesis, photophysical properties and TD-DFT calculation offour two-photon absorbing triphenylamine derivatives. Sci. ChinaChem. 56, 106–116.
Fang, W., Zhang, Y., Zhang, G., Kong, L., Yang, L., Yang, J., 2017. Multi-stimuli-responsive fluorescence of a highly emissive difluoroboron complex in both solution and solid states. CrystEngComm 19 (9), 1294–1303.
M.J. Frisch, G.W. Trucks, H.B. Schlegel, G.E. Scuseria, M.A. Robb, J.R. Cheeseman, G. Scalmani, V. Barone, B. Mennucci, G.A. Petersson, H. Nakatsuji, M. Caricato, X. Li, H.P. Hratchian, A.F. Izmaylov, J. Bloino, G. Zheng, J.L. Sonnenberg, M. Hada, M. Ehara, K. Toyota, R. Fukuda, J. Hasegawa, M. Ishida, T. Nakajima, Y. Honda, O. Kitao, H. Nakai, T. Vreven, J.A. Montgomery Jr., J.E. Peralta, F. Ogliaro, M. Bearpark, J.J. Heyd, E. Brothers, K.N. Kudin, V.N. Staroverov, R. Kobayashi, J. Normand, K. Raghavachari, A. Rendell, J.C. Burant, S.S. Iyengar, J. Tomasi, M. Cossi, N. Rega, J.M. Millam, M. Klene, J.E. Knox, J.B. Cross, V. Bakken, C. Adamo, J. Jaramillo, R. Gomperts, R.E. Stratmann, O. Yazyev, A.J. Austin, R. Cammi, C. Pomelli, J.W. Ochterski, R.L. Martin, K. Morokuma, V.G. Zakrzewski, G.A. Voth, P. Salvador, J.J. Dannenberg, S. Dapprich, A.D. Daniels, O. Farkas, J.B. Foresman, J.V. Ortiz, J. Cioslowski, D.J. Fox, Gaussian 09, Revision A. 1, Gaussian Inc., Wallingford CT 2009.
Zhang, Y.Y., Ma, Y.Q., Kong, L., Tian, Y.P., Yang, J.X., 2018. A novel indolo [3,2-b] carbazole derivative with D-π-A structure exhibiting aggregation-enhanced emission and mechanofluorochromic properties. Dyes Pigments 159, 314–321.
Bucinskas, A., Bagdziunas, G., Tomkeviciene, A., Volynyuk, D., Kostiv, N., Gudeika, D., Jankauskas, V., Rutkis, M., Grazulevicius, J.V., 2015. Structure-property relationship of isomeric diphenylethenyl-disubstituted dimethoxycarbazoles. RSC Adv. 5 (61), 49577–49589.
Galer, P., Korošec, R.C., Vidmar, M., Šket, B., 2014. Crystal structures and emission properties of the BF_2 complex 1-phenyl-3-(3,5-dimethoxyphenyl)-propane-1,3-dione: multiple chromisms, aggregation-or crystallization-induced emission, and the self-assembly effect. J. Am. Chem. Soc. 136, 7383–7394.
Hu, R., Lager, E., Aguilar-Aguilar, A., Liu, J., Lam, J.W.Y., Sung, H.H.Y., Williams, I.D., Zhong, Y., Wong, K.S., Peña-Cabrera, E., Tang, B.Z., 2009. Twisted intramolecular charge transfer and aggregation-induced emission of BODIPY derivatives. J. Phys. Chem. C 113 (36), 15845–15853.
Zheng, H., Ye, H.B., Yu, X.X., You, L., 2019. Interplay between n→π* interactions and dynamic covalent bonds: quantification and modulation by solvent effects. J. Am. Chem. Soc. 141, 8825–8833.
Feng, Z.L., Jia, S.P., Chen, H., You, L., 2020. Modulation of imine chemistry with intramolecular hydrogen bonding: effects from ortho-OH to NH. Tetrahedron 76, 131128.
Evecen, M., Duru, G., Tanak, H., Ağar, A.A., 2016. Synthesis, crystal structure, spectral analysis and DFT computational studies on a novel isoindoline derivative. J. Mol. Struct. 1118, 1–9.
Awuah, S.G., Polreis, J., Biradar, V., You, Y., 2011. Singlet oxygen generation by novel NIR BODIPY dyes. Org. Lett. 13 (15), 3884–3887.
Hariharan, P.S., Venkataramanan, N.S., Moon, D., Anthony, S.P., 2015. Self-reversible mechanochromism and thermochromism of a triphenylamine-based molecule: tunable fluorescence and nanofabrication studies. J. Phys. Chem. C 119, 9460–9469.
Yang, Z.Y., Qin, W., Lam, J.W.Y., Chen, S.J., Sung, H.H.Y., Williams, I.D., Tang, B.Z., 2013. Fluorescent pH sensor constructed from a heteroatom-containing luminogen with tunable AIE and ICTcharacteristics. Chem. Sci. 4, 3725–3730.
Jiménez-Sánchez, A., Farfán, N., Santillan, R., 2015. Multiresponsive photo-, solvato-, acido-, and ionochromic schiff Base probe. J. Phys. Chem. C 119 (24), 13814–13826.
Wu, D.B., Gong, W.J., Yao, H.M., Huang, L.M., Lin, Z.H., Ling, Q.D., 2020. Highly efficient solid-state emission of diphenylfumaronitriles with full-color ATE, and application in explosive sensing, data storage and WLEDs. Dyes Pigments 172, 107829.
Wang, A.W., Hou, Y.L., Kang, F.W., Lyu, F., Xiong, Y., Chen, W.C., Lee, C.S., Xu, Z.T., Rogach, A.L., Lu, J., Li, Y.Y., 2019. Rare earth-free composites of carbon dots/metal-organic frameworks as white light-emitting phosphors. J. Mater. Chem. C 7, 2207–2211.